for the ratio of Mg (in grams per kilogram of seawater) to Cl (in parts per thousand), then $[Mg^{2+}]$ is also known as a function of salinity. Finally, K_c depends on μ and hence on S; its dependence has been determined by Cheek (*9*).

If we combine Eqs. 5 and 7 and note that $C_{F^-} = [F^-] + [MgF^+] = [F^-](1 + K_c[Mg^{2+}])$, the relation between the fluoride activity sensed by the electrode in the buffered solution and the total inorganic fluoride in the sample before dilution C_{F^-} is given by a function $K_a(S)$ which depends only on salinity

$$C_{F^-} = a_{F^-} \left(\frac{w + v}{v}\right) \frac{(1 + K_c\,[Mg^{2+}])}{\gamma_{F^-}} \quad (8)$$

Thus

$$C_{F^-} = a_{F^-} K_a\,(S) \quad (9)$$

where K_c, γ_{F^-}, and $[Mg^{2+}]$ all pertain to the sample after addition of buffer, that is, at some new ionic strength μ_{mix} and lower $[Mg^{2+}]$.

When salinities of the standard and of the unknown are the same, K_a is a constant, and, based on a comparison of Eqs. 1, 4, and 9

$$\beta = \alpha + (RT/\mathbf{F}) \ln K_a$$

When $S_1 \neq S_2$, β is not constant and is given by

$$\beta = \alpha + (RT/\mathbf{F}) \ln K_a(S_1)$$

in the standardizing solution, but in the unknown by

$$\beta = \alpha + (RT/\mathbf{F}) \ln K_a(S_2)$$

Rather than use the absolute values of $K_a(S)$, it is convenient to assume a constant value of β and to apply the correction after computing the approximate concentration C_x, as in Eq. 2, and then to apply the correction in Eq. 3, where

$$Q_a(S) = K_a(S_2)/K_a(S_1) \quad (10)$$

The function $Q_a(S)$ changes slowly with salinity, and, because this function is a quotient, it is important that slopes be known; however, $Q_a(S)$ is insensitive to errors in the absolute magnitudes of the quantities that determine $K_a(S)$.

Values of $Q_a(S)$, calculated from Eqs. 8 through 10, are given in Table 1. An effective γ (including contributions from the liquid junction potential) was experimentally measured at $\mu_{mix} = 0.900$; γ at other values of μ_{mix} was calculated from existing $d\gamma/d\mu$ data. The calculated and experimental values of Q_a (Fig. 1) are in good agreement. They differ by no more than 0.002 for $32 < S_2 < 37$ parts per thousand; the maximum deviation in $Q_{a,calc}$ is -0.008 at $S_2 = 38.9$ parts per thousand and $+0.004$ at $S_2 = 30$ parts per thousand. The calculated values are reproduced to within 0.004 by

$$Q_a(S) = (\text{salinity}/57.9) + 0.408$$

Similar values of Q_a can be computed for other values of S_1, v, w, and μ_1, if necessary.

Error in fluoride determinations is primarily due to the drift of standardization with time. Stability and reproducibility of electrode response is shown in Fig. 2 for samples of synthetic seawater of constant salinity (*3*) maintained at 25.0°C. In each run the electrodes were standardized just once, and concentrations in other samples were computed on the assumption of a Nernstian response. The difference between measured and known C_{F^-} was expressed as the percentage of relative error. The relative standard deviation of an individual measurement from the true value was 1.2 percent, based on 45 measurements, and mean deviation was -0.4 percent. Real seawater (salinity = 36.12 parts per thousand, C_{F^-} = 74.3 μmole/liter) spiked with additional fluoride yielded a relative standard deviation of the measured fluoride from true fluoride of 0.6 percent based on five measurements between 74 and 183 μmole/liter. Analysis of the data (Fig. 1) indicates that uncertainties involved in the use of Eq. 3 do not materially degrade precision when experimental values of Q_a are used. For 25 determinations the relative standard deviation of an individual measurement was 0.2 percent. Accuracy of concentrations inferred in natural waters depends on the validity of the CCSW assumption. If we combine the above errors with the probable maximum variation in the ratio of Mg to Cl, the limits of relative error for measurements in real waters having variable salinity may be taken as about 5 percent. For atypical waters the technique cannot be used without additional data.

The validity of Eqs. 1 through 3 was verified by determining C_{F^-} in a single sample of Atlantic seawater (salinity 36.15 parts per thousand) by two independent methods. Photon activation analysis (*10*) indicated a fluoride concentration of 1.35 ± 0.18 μg/ml; with the LaF_3 electrode, the concentration found was 1.41 ± 0.07 μg/ml, both errors being limits of error.

THEODORE B. WARNER
Naval Research Laboratory, Washington, D.C. 20390

References and Notes

1. R. Greenhalgh and J. P. Riley, *Nature* **197**, 371 (1963).
2. M. S. Frant and J. W. Ross, Jr., *Anal. Chem.* **40**, 1169 (1968).
3. J. Lyman and R. H. Fleming, *J. Mar. Res.* **3**, 134 (1940).
4. M. S. Frant and J. W. Ross, Jr., *Science* **154**, 1553 (1966).
5. T. B. Warner, *Anal. Chem.* **41**, 527 (1969).
6. F. Culkin, in *Chemical Oceanography*, J. P. Riley and G. Skirrow, Eds. (Academic Press, New York, 1965), pp. 125 and 143.
7. Orion Research, Inc., instruction manual, ed. 2, for fluoride ion activity electrode model 94-09 (1967).
8. M. E. Thompson, *Science* **153**, 866 (1966); R. M. Pytkowicz and R. Gates, *ibid.* **161**, 690 (1968).
9. C. H. Cheek, personal communication.
10. P. E. Wilkniss and V. J. Linnenbom, *Limnol. Oceanogr.* **13**, 530 (1968).
11. I thank P. E. Wilkniss for the sample of Atlantic seawater and results of activation analysis, R. A. Carr for the Mediterranean sample, and C. H. Cheek for making his results on K_c as a function of ionic strength available prior to publication.

25 November 1968; revised 10 April 1969

Water Vapor: Observations of Galactic Sources

Abstract. *We measured the emission of water vapor at a wavelength of 1.35 centimeters from nine sources with the 120-foot (36.5-meter) Haystack antenna. Eight sources lie within 30 seconds of arc of the hydroxyl sources of 18 centimeters but not all hydroxyl sources produced detectable emission of water vapor. All sources are smaller than 30 seconds of arc in angular diameter, but we resolved at least three separate sources in the Orion Nebula. We do not find that the known hyperfine components are present with the equilibrium intensity distribution.*

Microwave emission by interstellar water vapor by virtue of the rotational transition at a wavelength of 1.35 cm has been discovered by Cheung *et al.* (*1*) and further studied by Knowles *et al.* (*2*). We now report independent observations of the emission by interstellar H_2O which confirm and extend the previous results. Our observations show that (i) the emission from the Orion

Nebula originates from at least three separate sources; (ii) the emission from the HII region in W49 extends over 280 km/sec in Doppler velocity; (iii) appreciable H_2O emission occurs from the position of the maximum in the W3 thermal continuum at velocities of approximately -40 to $+20$ km/sec; (iv) the OH emission source NGC 6334N is also a source of H_2O emission; and (v) comparison of our spectra with those of Knowles *et al.* (*2*) suggests that emission from G133.7 + 1.2, VY Canis Majoris, and the Orion Nebula may have changed in an interval of 1 or 2 months.

The frequencies of hyperfine components of the water-vapor transition (*3*) are separated by intervals that are not much less than the widths of observed emission features. We attempted unsuccessfully to fit the equilibrium distribution of component intensities to the shape of an observed feature with very high signal-to-noise ratio. A single Gaussian profile gives a better fit to the data above the half-power level. Several hyperfine components may in fact be present with nonequilibrium intensity ratios, but the identification of specific hyperfine components in the observed spectra is uncertain.

We observed with the 120-foot (36.5-m) Haystack antenna of M.I.T. Lincoln Laboratory during the period from 7 February 1969 to 10 March 1969. We used a superheterodyne receiver switched between two horn feeds, one on the antenna axis and the other offset in azimuth by 4.5 minutes of arc. The system temperature was 4600°K for dual side-band operation. Spectra were observed with a digital autocorrelation system described by Ball and Meeks (*4*). We used spectrometer bandwidths of 4 Mhz, 1.2 Mhz, 400 khz, and 120 khz. For each bandwidth the frequency resolution was equivalent to a filter width (between half-power points) of 1/40 the spectrometer bandwidth. The spurious response of the spectrometer was less than 3 percent.

The two feed horns were linearly polarized with the electric vector in the vertical plane for the on-axis feed and in the horizontal plane for the off-axis feed. A quarter-wave plate could be mounted in front of the on-axis horn for right or left circular polarization.

At the wavelength of the water-vapor transition, 1.35 cm, the antenna beam width between half-power points is 1.5 minutes of arc. We determined the beam width by scanning across the planet Venus in right ascension and declination and correcting the apparent widths for the finite angular size of the source. The pointing errors of the Haystack antenna after calibration at a wavelength of 2 cm have been reported by Meeks *et al.* (*5*). The residual pointing errors had root-mean-square values of 10 seconds of arc in azimuth and 12 seconds of arc in elevation. During the observations reported here we found the pointing reproducible from day to day with accuracies consistent with these residual errors. Corrections for atmospheric refraction were made on the basis of surface values of temperature and relative humidity.

We searched for water-vapor emis-

Table 1. Successful searches for water vapor: search parameters, detection limits, and other line observations.

Source name	Other lines observed	Radial velocity V_R of observed lines (km/sec)	Reference	V_R search interval (km/sec)	Antenna temperature T_A limit* (°K)
W3 continuum (G133.7 + 1.2)	H recombination	-42.3	(*4*)	-65 to $+35$	25
W3 OH	OH	-48 to -40	(*15*)	-150 to $+370$	20
Orion Nebula	OH	-8 to $+23$	(*16*)	-20 to $+35$	20
VY Canis Majoris	OH	-14 to $+58$	(*8*)	-172 to $+128$	25
Sgr B2 (G0.7 − 0.0)	OH	50 to 77	(*17*)	27 to 114	30
NGC 6334 (N)	OH	-14 to -7	(*9*)	-94 to $+67$	25
W49 (position 1)	OH	0 to 22	(*9*)	-180 to $+160$	25
W51	OH	57 to 63	(*9*)	$+30$ to $+130$	15
W75 (S)	OH	-1 to $+6$	(*9*)	-125 to $+191$	30

* Corrected for elevation-angle dependence.

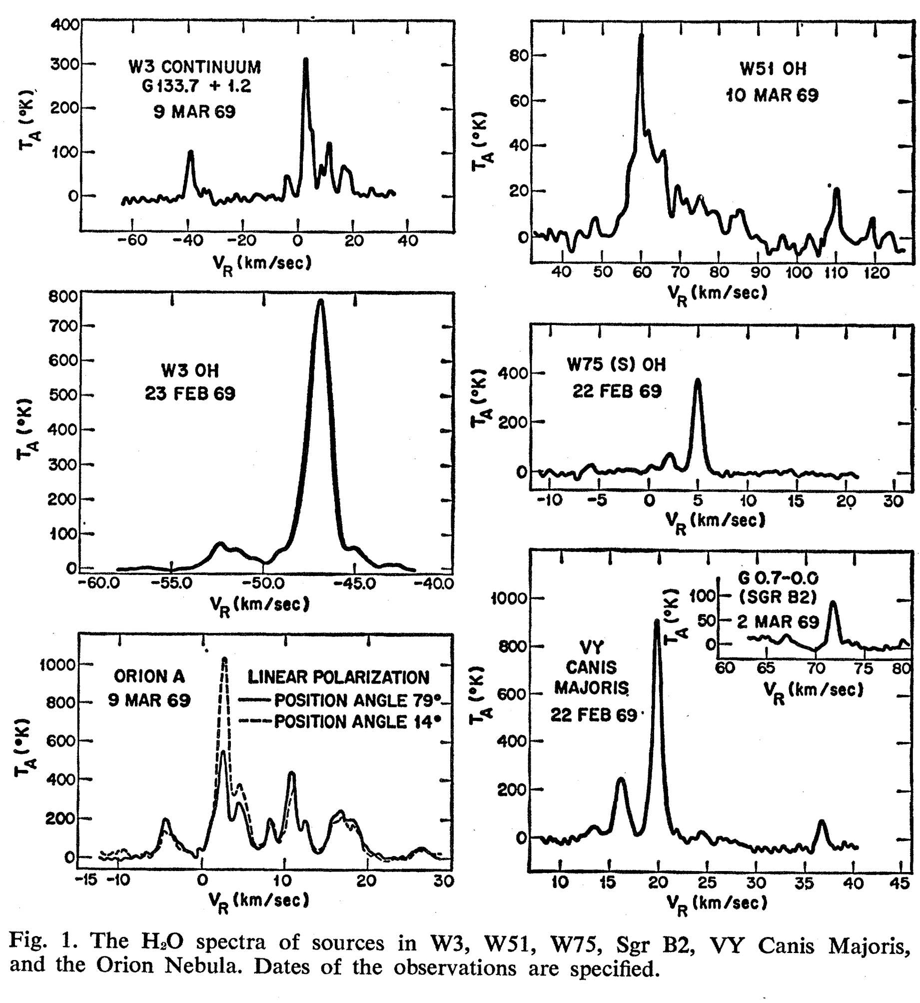

Fig. 1. The H_2O spectra of sources in W3, W51, W75, Sgr B2, VY Canis Majoris, and the Orion Nebula. Dates of the observations are specified.

Table 2. Source positions in the Orion Nebula.

Radial velocity (km/sec)	Right ascension offset (seconds of arc)*	Declination offset (seconds of arc)*
−4.0	0(± 7)	0(± 7)
3.0	−18(± 4)	14(± 4)
5.0	−18(± 7)	14(± 7)
8.7	0(± 8)	7(± 8)
11.4	0(± 4)	0(± 4)
16.4	−7(± 7)	2(± 7)
18.5	0(± 7)	0(± 7)
27.0	−18(± 10)	−18(± 10)

* Offsets are measured from the position of the feature at 11.4 km/sec that appears to coincide with the OH-source position. The errors in parentheses represent our best estimate of the uncertainties in the offsets.

sion primarily at positions where intense OH emission has been observed. Precise positions of several OH sources have been measured with two-element interferometers by Cudaback *et al.* (*6*), Rogers *et al.* (*7*), Eliasson and Bartlett (*8*), and Raimond and Eliasson (*9*). We searched at ten OH-source positions measured to within a few seconds of arc (*8, 9*). At eight of these positions we observed H_2O emission. We know of only one case of an H_2O source detected at a position that does not correspond to a precisely known OH-source position. In this latter case, H_2O emission is associated with the thermal radio source G133.7 + 1.2, near W3 OH.

We can make several general statements about the sources observed:

First, the positions of OH and H_2O sources agree to within the accuracy of our antenna pointing calibration. The observed offsets were in every case less than 30 seconds of arc. Second, the angular size of all emission features appeared to be small compared to the antenna beam width (less than 30 seconds of arc) because no beam-broadening was observed. However, the H_2O source in the Orion Nebula was resolved into three separate emission points. Third, we observed polarization only in the H_2O emission from Orion A; this shows a high degree of linear polarization. However, we were unable to distinguish degrees of polarization of the order of 10 percent or less because our feed arrangement required comparison of spectra obtained with separate observations. We have corrected the antenna temperature scales of our spectra for an atmospheric attenuation given by $\tau_0 \sec \theta$, where τ_0 is the zenith attenuation and θ is the zenith angle. On a typical clear day, we measured a value of $\tau_0 = 0.75$ db from observations of VY Canis Majoris between zenith angles of 70° and 82°. This value of τ_0 includes the effect of gain change with elevation as well as atmospheric attenuation.

With the exception of sources W49 and NGC 6334, all of the water-vapor emission that we observed is shown in Fig. 1. The radial-velocity scales here are specified with respect to the local standard of rest on the basis of an assumed frequency of 22.23522 Ghz. In most cases, we searched over much wider intervals of radial velocity than shown in Fig. 1. The intervals searched and the detection limits are listed in Table 1 for all sources in which we observed emission. This table also contains radial velocities for OH or hydrogen-recombination emission from these sources. Generally, H_2O emission overlaps that from other spectral lines but there is no detailed correspondence in the spectra.

Our most nearly noise-free spectrum was obtained for W3 OH. This spectrum is in good agreement with measurements by Knowles *et al.* (*2*), and our peak temperature is nearly identical with theirs (*10*). We have used this profile for detailed considerations of line shape. Spectra from the brightest continuum radio source in the W3 region, designated by its galactic coordinates (in degrees) as G133.7 + 1.2, do not agree with those of Knowles *et al.* (*2*). The profiles are similar for the radial-velocity interval from −43 to −30 km/sec, but our antenna temperatures are smaller by a factor of ½. Furthermore, the features in the velocity interval from −5 to +20 km/sec (Fig. 1) were not reported by Knowles *et al.* (*2*). Our observations of the infrared source VY Canis Majoris are in agreement with those of Knowles *et al.* (*2*), from 15 to 25 km/sec, but the feature at 37 km/sec has not been detected previously. We found H_2O emission from NGC 6334 at −3 km/sec with an antenna temperature (corrected for dependence on the elevation angle) of 45°K. This source coincides with the northernmost member of the pair of OH sources in this nebula. Observation of this region is difficult at our latitude because the source transits at an elevation angle of 12°. We found only one feature in G0.7 − 0.0 rather than the two previously reported (*2*). We cannot rule out the possibility that the second feature is at a slightly different position (*9*).

Our spectrum for W51 (Fig. 1) fails to resolve the emission between 55 and

Table 3. Unsuccessful searches for water vapor: search parameters and detection limits.

Source name	Right ascension α (1950.0)	Declination δ (1950.0)	Radial velocity V_R interval (km/sec)	Antenna temperature T_A limit (°K)	Search dates (1969)
Tau A	$5^h31^m30^s$ (searched ± 5^s)	21°59′00″ (searched ± 70″)	−26 to 67	20	2/10, 3/1
W12	$5^h39^m12^s$ (searched ± 7^s)	−1°55′42″ (searched ± 100″)	−26 to 26	40	2/15
R-Mon	$6^h36^m26^s$	8°47′27″	−54 to 54	20	2/16
IR1013 + 30	$10^h13^m18^s$	30°49′00″	−80 to 80	20	2/16, 2/22
R-Cor Bor	$15^h46^m31^s$	28°18′32″	−87 to 87	20	2/16
NGC 6334 (S)	$17^h16^m36^s$	−35°54′57″	−26 to 26	10	2/15, 3/2
Sgr A (NH_3)	$17^h42^m27^s$ (searched ± 8^s)	−29°01′00″ (searched ± 100″)	−25 to 48	20	3/2
W28 (S)	$17^h57^m30^s$	−24°04′30″	−57 to 57	10	2/15
W28 (N)	$17^h58^m52^s$	−23°17′30″	26 to 53	10	2/15
W33	$18^h11^m42^s$ (searched ± 15^s)	−17°53′48″ (searched ± 240″)	18 to 72	20	2/15, 3/10
W40	$18^h28^m51^s$	− 2°07′29″	−26 to 26	20	2/13
W43	$18^h45^m01^s$ (searched ± 7^s)	− 2°00′03″ (searched ± 100″)	64 to 117	20	2/13
W44	$18^h54^m02^s$	1°23′24″	−26 to 66	20	2/13
IR1903 + 08	$19^h03^m58^s$	8°09′06″	76 to 26	20	2/13
W75 (N)	$20^h36^m51^s$ (searched ± 14^s)	42°25′30″ (searched ± 150″)	−25 to 77	20	2/13
IR2041 + 43	$20^h41^m36^s$	43°01′00″	−134 to 26	20	2/29
NML-Cyg	$20^h44^m34^s$ (searched ± 5^s)	39°55′57″ (searched ± 70″)	−54 to 86	20	2/13, 2/28, 3/1
Venus	~ 0^h50^m	~ 9°	−26 to 26*	20	2/13
Jupiter	~ 12^h19^m	~ 0°	−26 to 26*	20	2/10

* Radial velocities with respect to the planet barycenters.

68 km/sec. Observations with higher resolution show five distinct peaks between 57 and 67 km/sec. We observed the OH source W75 (S), near the compact HII region in DR21 (*11*), and obtained water-vapor spectra that are in good agreement in profile and antenna temperature with those reported by Knowles *et al.* (*2*). The discrepancies between our spectra from G133.7 + 1.2 and VY Canis Majoris and those of Knowles *et al.* (*2*) may be the result of intrinsic time variations.

We observed the Orion Nebula with circular polarization at a grid of points spaced at intervals of 45 seconds of arc and extending ± 1.5 minutes of arc in right ascension and declination from the position of the OH source. These observations disclosed three distinct emission points. Table 2 shows the results of an analysis of these spectra at eight different radial velocities. On the basis of estimated errors in Table 2, we judge that emission at −4.0, 8.7, 11.4, 16.4, and 18.5 km/sec originates from a common point. This point appears to coincide with the OH source and the coincident infrared point source of Becklin and Neugebauer (*12*). The emission at 3.0 and 5.0 km/sec comes from a second point 25 seconds of arc away. The emission at 27.0 km/sec originates at a third point 34 seconds of arc south of the second source point. Infrared observations by Ney and Allen (*12*) at 11.6 and 20 μm indicate that infrared emission is associated with all three of the H_2O source positions. However, we must point out the discrepancy between the angular structure we observed in this source and the results of Knowles *et al.* (*2*), who report these features coincident to within 0.1 minute of arc. Figure 1 shows H_2O spectra from the Orion Nebula taken with linear polarization. Linear polarization with several different position angles is evidently present, and the polarization of the brightest feature is about 30 percent. A comparison of our spectra with those of Knowles *et al.* (*2*) shows evidence of time variation around a radial velocity of 2 km/sec.

There are two OH-source points in the W49 region, designated positions 1 and 2 and separated by 2.4 minutes of arc. We report emission only from position 1. We detected emission features beginning at a radial velocity of − 140 km/sec and extending to + 140 km/sec, but we observed the central part of this radial-velocity interval most frequently. Figure 2 shows that time variations are evident in the interval from −15 to + 40 km/sec. All features in this interval are coincident in position within ± 10 seconds of arc and their degree of polarization is less than 10 percent. The spectra (Fig. 2) were observed at intervals of about a week at various elevation angles and under various weather conditions (*13*). We have arbitrarily adjusted the antenna temperature scales so that the brightest feature at 12 km/sec remains constant. Progressive changes are apparent in the shapes of several features: between − 8 and + 3 km/sec the brightest feature is decreasing in intensity and the adjacent feature on the right is increasing (*14*); the peaks at 14.5, 21, and 27 km/sec are decreasing. Our data for 10 February 1969 are in good agreement with the spectrum of Knowles *et al.* (*2*) for 8 February 1969.

Table 4. Hyperfine components of the $6_{16} \rightarrow 5_{23}$ transition of H_2O; *F* and *F'* are the total angular momentum quantum numbers in the initial and final states.

F	*F'*	Measured frequency (khz)	Relative intensity (%)
7	6	22,235,044.66 ± 0.1	38.5
6	5	22,235,077.70 ± 0.1	32.4
5	4	22,235,120.86 ± 0.1	27.3
6	6	22,235,253.3 ± 1.5	0.9
5	5	22,235,298.5 ± 1.2	0.9

We measured the high negative velocity from − 140 to − 10 km/sec of 16 February, 2 March, and 8 March, and we found no changes in the 23 features that were found in this radial-velocity interval observed with 100-khz resolution. The high positive-velocity spectrum from 30 to 140 km/sec showed fewer features, but time variations were observed in a feature at 140 km/sec. This feature gave a peak antenna temperature of 400°K on 16 February. It had been discovered first on 12 February but no emission could be detected on 9 March.

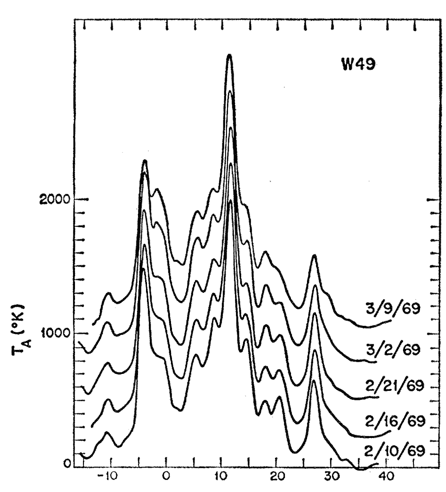

Fig. 2. The H_2O spectra of W49 (position 1): central range of radial velocities observed on five different days; *VLSR* represents the velocity with respect to the local standard of rest. The intensities are normalized on the most intense feature at 12 km/sec, and the spectra are superimposed to show progressive time variations. The resolution is 100 khz (or 1.5 km/sec).

We searched for H_2O emission and absorption in 20 other sources without success. Table 3 lists these sources and the relevant search parameters.

We also searched for the 22.3077-Ghz rotational transition of HDO. This transition involves the asymmetric-top states 5_{32} and 5_{33}. We observed at the positions and radial velocities of the most intense H_2O emission from W3 OH, W49, W75, and Orion A. Our detection limit was an antenna temperature of ± 2°K on all sources except Orion A where the limit was 6°K. For the most intense H_2O feature that we observed, W49 at 12 km/sec, the upper limit for HDO is 1/1000 times the H_2O intensity.

The H_2O rotational states involved in the transition are split by interaction between the nuclear spins of the hydrogen atoms and the rotational angular momentum of the molecule. Because of symmetry considerations, the quantum number for nuclear spin *I* is restricted to $I = 1$. Although the magnetic spin–rotational coupling is comparatively weak, the resulting hyperfine splitting must be taken into account because of the narrow line widths observed. The hyperfine structure of the transition from 6_{16} to 5_{23} in H_2O has been measured by Bluyssen *et al.* (*3*). We give in Table 4 the frequencies of these transitions and the relative intensities (as percentages of the total intensity summed over all hyperfine components). These intensities apply to an equilibrium distribution of state populations. The transitions from 6 to 6 and 5 to 5 are weaker than the other three transitions by a factor of about 30. The separations between the most intense transitions are 33.04 and 43.16 khz in order of increasing transition frequency. Accordingly, we would expect the hyperfine splitting to affect line shape rather than to produce separate features in the emission spectra. We attempted to fit the shape of the feature at 47 km/sec from the position W3 OH (Fig. 1) by assuming the intensities and line spacings in Table 4 and taking various (equal) line widths and Gaussian profiles for the transitions. We were unable to obtain a satisfactory fit in this way. Hence, we may conclude, independent of considerations of source-brightness and polarization, that we are not observing a source in thermal equilibrium. A single Gaussian profile is an excellent fit to the feature profile above the half-maximum level, but below this level the observed profile is broader than the Gaussian profile, particularly on the low-velocity (high-frequency) side. However, we estimate that these features could be fitted very accurately if we relaxed the constraint that the three most intense transitions in Table 4 have the equilibrium intensity ratios. The high observed antenna temperatures and the small angular size of the regions of water emission imply high brightness temperatures and suggest a maser-type emission. The relative intensities could, in fact, be altered by the ratios of the maser gains for various hyperfine transitions, but we cannot distinguish between saturated and exponential gains on the basis of these data. Nevertheless, the presence of hyperfine splitting must be taken into account if we are to interpret the apparent feature widths.

M. L. MEEKS
J. C. CARTER
Lincoln Laboratory, Massachusetts Institute of Technology, Lexington
A. H. BARRETT
P. R. SCHWARTZ, J. W. WATERS
Department of Physics and Electrical Engineering and *Research Laboratory of Electronics, Massachusetts Institute of Technology, Cambridge*
W. E. BROWN III
Optics and Microwave Laboratory, Electronics Research Center, National Aeronautics and Space Administration, Cambridge, Massachusetts 02139

References and Notes

1. A. C. Cheung, D. M. Rank, C. H. Townes, D. D. Thorton, W. J. Welch, *Nature* **221**, 626 (1969).
2. S. H. Knowles, C. H. Mayer, A. C. Cheung, D. M. Rank, C. H. Townes, *Science* **163**, 1055 (1969); *ibid.* **164**, 57 (1969). The antenna temperature in their Orion spectrum is high by a factor of 2.
3. H. Bluyssen, A. Dymanus, J. Verhoeven, *Phys. Lett.* **24A**, 482 (1967).
4. J. A. Ball and M. L. Meeks, *Astrophys. J.* **153**, 577 (1968); E. C. Reifenstein, thesis, Massachusetts Institute of Technology (1968).
5. M. L. Meeks, J. A. Ball, A. B. Hull, *IEEE (Inst. Elec. Electron. Eng.) Trans. Antennas Propagation* **AP-16**, 746 (1968).
6. D. D. Cudaback, R. B. Read, G. W. Rougoor, *Phys. Rev. Lett.* **17**, 452 (1966).
7. A. E. E. Rogers, J. M. Moran, P. P. Crowther, B. F. Burke, M. L. Meeks, J. A. Ball, G. M. Hyde, *Astrophys. J.* **147**, 369 (1967).
8. B. Eliasson and J. F. Bartlett, *ibid.* **155**, L79 (1969).
9. E. Raimond and B. Eliasson, *ibid.*, p. 817. The OH source near Sgr B2 was reported to consist of two points: (i) a source of 1665- and 1667-Mhz emission, and (ii) a much weaker source of 1665-Mhz emission lying 36 seconds of arc north of the principal source point. We found H_2O emission coinciding in position with (i).
10. The effective area of the Haystack antenna at a wavelength of 1.35 cm appears to be approximately equal to that of the 85-foot (26-m) antenna of the Naval Research Laboratory (*2*). We believe the surface tolerance of these two antennas is nearly equal because the predicted loss from the Haystack radome at this wavelength (2.4 db) approximately offsets the difference in diameter. The half-power beam widths, of course, scale as 85:120.
11. M. Ryle and D. Downs, *Astrophys. J.* **148**, L17 (1967).
12. E. E. Becklin and G. Neugebauer, *ibid.* **147**, 799 (1967); E. P. Ney and D. A. Allen, *ibid.* **155**, L193 (1969).
13. Weather conditions during the observations on 10 February 1969 were unusually bad. The W49 spectrum shown for that date in Fig. 2 was taken during the worst Boston-area blizzard in 20 years.
14. Initial observations of this source with the National Radio Astronomy Observatory 140-foot (42.7-m) antenna on 8 to 16 April 1969 by A.H.B., J.W.W., and P.R.S. show these changes to be continuing with three distinct peaks showing up in this radial-velocity interval.
15. M. L. Meeks, J. A. Ball, J. C. Carter, R. P. Ingalls, *Science* **153**, 978 (1966).
16. T. K. Menon, *Astrophys. J.* **150**, L167 (1967).
17. P. Palmer and B. Zuckerman, *ibid.* **148**, 727 (1967).
18. For observing assistance we thank A. E. E. Rogers, P. Rosenkrantz, W. J. Wilson, and C. A. Zapata. We are grateful to J. A. Ball, M. M. Litvak, and P. Thaddeus for helpful discussions, and to G. G. Haroules for engineering assistance. The radiometer was provided on loan by the Electronics Research Center, National Aeronautics and Space Administration, Cambridge, Massachusetts. Sponsored in part by the U.S. Air Force (M.I.T. Lincoln Laboratory) and by NASA grant NGL 22-009-016.

25 April 1969; revised 12 June 1969

Primary Afferent Depolarization Evoked by a Painful Stimulus

Abstract. *Pulses of intense radiant heat applied to the plantar pad of unanesthetized spinal cats produced negative dorsal root potentials, increased excitability of cutaneous A fibers, and marked activation of ipsilateral flexor motoneurons. The same effects were obtained during cold block of A fiber conduction in the appropriate peripheral nerve. We conclude that adequate noxious activation of cutaneous C fibers depolarizes cutaneous A fibers.*

A basic tenet in the theory of pain mechanisms proposed by Melzack and Wall (*1*) is that cutaneous afferent fibers of large and small diameter have opposing effects on the spinal mechanisms which presynaptically modulate synaptic transmission in other cutaneous afferents. This assumption was derived from the observation (*2*) that selective electrical stimulation of small-diameter unmyelinated cutaneous fibers (C fibers) produced positive dorsal root potentials (DRP's) and hypoexcitability of cutaneous afferent terminals. However, this is in conflict with studies (*3, 4*) which report that selective electrical C fiber stimulation resulted in negative DRP's similar to those produced by the large diameter myelinated A fibers from the skin.

Since electrical stimulation of skin nerves may not initiate patterns of afferent activity similar to those produced by natural painful stimuli, we have investigated the effects of intense radiant heat pulses applied to the plantar pad of spinal cats on the polarization of afferent fibers. This stimulus is clearly noxious and produces intense pain when applied to human skin, and the stimulus appears to activate primarily, if not exclusively, C fibers (*5*).

Under halothane anesthesia, the lumbosacral spinal cord of adult cats was exposed and sectioned at the first lumbar segment (L1). The ventral roots (VR) of L6 through S1 were cut and a small filament of the L6 dorsal root (DR) was cut and prepared for recording. All sciatic nerve branches were cut in the left leg except for the posterior tibial nerve, and some were placed on platinum wire electrodes. After completion of the dissection the animals were decerebrated and, with anesthesia discontinued, paralyzed with gallamine triethiodide and artificially respired. The cord and nerves were covered with warm mineral oil. Blood pressure and body temperature were monitored continuously and remained within normal limits. The posterior tibial nerve containing the afferents from the central plantar pad was preserved intact and in some experiments was mounted on a cooling device to block nerve conduction (*4*). Hair around the left central plantar pad was removed and a small thermocouple was placed on the pad surface for temperature recording. Pulses of radiant heat were directed exclusively to the pad by a focusing projection lamp covered with a movable shutter.

Intense heat pulses delivered to the plantar pad consistently evoked nega-